

Proton beam deflection in MRI fields: Implications for MRI-guided proton therapy

B. M. Oborn^{a)}

Illawarra Cancer Care Centre (ICCC), Wollongong, NSW 2500, Australia and Centre for Medical Radiation Physics (CMRP), University of Wollongong, Wollongong, NSW 2500, Australia

S. Dowdell

Shoalhaven Cancer Care Centre, Nowra, NSW 2541, Australia

P. E. Metcalfe

Centre for Medical Radiation Physics (CMRP), University of Wollongong, Wollongong, NSW 2500, Australia and Ingham Institute for Applied Medical Research, Liverpool, NSW 2170, Australia

S. Crozier

School of Information Technology and Electric Engineering, University of Queensland, St. Lucia, QLD 4072, Australia

R. Mohan

Department of Radiation Oncology, MD Anderson, Houston, Texas 77030

P. J. Keall

Sydney Medical School, University of Sydney, Sydney, NSW 2006, Australia and Ingham Institute for Applied Medical Research, Liverpool, NSW 2170, Australia

(Received 9 December 2014; revised 1 March 2015; accepted for publication 17 March 2015;
published 10 April 2015)

Purpose: This paper investigates, via magnetic modeling and Monte Carlo simulation, the ability to deliver proton beams to the treatment zone inside a split-bore MRI-guided proton therapy system.

Methods: Field maps from a split-bore 1 T MRI-Linac system are used as input to GEANT4 Monte Carlo simulations which model the trajectory of proton beams during their paths to the isocenter of the treatment area. Both inline (along the MRI bore) and perpendicular (through the split-bore gap) orientations are simulated. Monoenergetic parallel and diverging beams of energy 90, 195, and 300 MeV starting from 1.5 and 5 m above isocenter are modeled. A phase space file detailing a 2D calibration pattern is used to set the particle starting positions, and their spatial location as they cross isocenter is recorded. No beam scattering, collimation, or modulation of the proton beams is modeled.

Results: In the inline orientation, the radial symmetry of the solenoidal style fringe field acts to rotate the protons around the beam's central axis. For protons starting at 1.5 m from isocenter, this rotation is 19° (90 MeV) and 9.8° (300 MeV). A minor focusing toward the beam's central axis is also seen, but only significant, i.e., 2 mm shift at 150 mm off-axis, for 90 MeV protons. For the perpendicular orientation, the main MRI field and near fringe field act as the strongest to deflect the protons in a consistent direction. When starting from 1.5 m above isocenter shifts of 135 mm (90 MeV) and 65 mm (300 MeV) were observed. Further to this, off-axis protons are slightly deflected toward or away from the central axis in the direction perpendicular to the main deflection direction. This leads to a distortion of the phase space pattern, not just a shift. This distortion increases from zero at the central axis to 10 mm (90 MeV) and 5 mm (300 MeV) for a proton 150 mm off-axis. In both orientations, there is a small but subtle difference in the deflection and distortion pattern between protons fired parallel to the beam axis and those fired from a point source. This is indicative of the 3D spatially variant nature of the MRI fringe field.

Conclusions: For the first time, accurate magnetic and Monte Carlo modeling have been used to assess the transport of generic proton beams toward a 1 T split-bore MRI. Significant rotation is observed in the inline orientation, while more complex deflection and distortion are seen in the perpendicular orientation. The results of this study suggest that due to the complexity and energy-dependent nature of the magnetic deflection and distortion, the pencil beam scanning method will be the only choice for delivering a therapeutic proton beam inside a potential MRI-guided proton therapy system in either the inline or perpendicular orientation. Further to this, significant correction strategies will be required to account for the MRI fringe fields. © 2015 American Association of Physicists in Medicine. [<http://dx.doi.org/10.1118/1.4916661>]

Key words: MRI-proton therapy, proton beam, magnetic field, Monte Carlo simulation, magnetic deflection

1. INTRODUCTION

MRI-guided radiotherapy has fast become a topic of interest in the field of medical physics research. The promise of high quality real-time MR-images of a changing patient anatomy, coupled with a dynamic radiation beam delivery, is the clear advantageous end goal of this modality. At present, clinical treatments have been reported for the related and less complex MRI-cobalt system,¹ but not for a Linac based system. Current MRI-Linac based programs include a 1.5 T, 6 MV second-generation system at UMC Utrecht,² a second-generation 0.56 T, 6MV design at the University of Alberta,³ and a new 1 T split-bore 6MV system (under construction) at the Ingham Institute, Sydney, Australia.⁴ The mechanical and design hurdles overcome to bring these two systems together has been well documented in the literature and is still active. Electron gun and/or waveguide operation and shielding has been investigated by various authors.^{5–9} MLC motor operation and impact on MRI uniformity have been studied.^{10,11} MRI magnet and coil design have been presented.^{12–15} Radiofrequency interference between the MRI and Linac has also been studied.^{16,17} The various dosimetry changes caused by the magnetic fields are also described, including both transverse^{18–27} and longitudinal magnetic fields.^{22,28–30} The performance of common radiation detectors in magnetic fields has also been investigated.^{31–35}

Contrary to working prototypes, MRI-guided proton beam therapy has only been described in simulations or general discussions. This hypothetical modality could, in theory, couple MRI guidance with the well known and often desirable characteristics of proton beams. Further to this, it could be argued that MR-guidance is more important for protons than photons as they are more sensitive to anatomical variations. There are obvious physical problems however with this modality: the charged proton beam will undergo deflections by the MRI magnetic field. To the best of our knowledge, only three specific studies exist with the main theme related to MRI-proton therapy. In the first study by Raaymakers *et al.*³⁶ in 2008, the dose changes in a water phantom, irradiated by a 90 MeV proton beam in the presence of a 0.5 and 3 T perpendicular fields, were simulated using conventional Monte Carlo methods. These fields were intended to represent the magnetic field where the patient or phantom would lie, namely, the MRI imaging field which is highly uniform in both direction and magnitude. It was discussed that the fringe field of the MRI would potentially slightly change the path of the proton beam before arriving at the patient surface. A suggested solution was to include a small extra gantry rotation or translation to correct for this effect. In the second paper by Wolf and Bortfeld,³⁷ a numerical solution was developed to predict the Bragg peak deflection of a proton beam traversing a water phantom in magnetic fields. This work described a similar match to the first work by Raaymakers *et al.* at 90 MeV, however further calculations were performed showing that at 200 MeV, the proton beam deflection is much stronger within a water phantom, but still predictable.

In the third and most recent work by Moteabbed *et al.*³⁸ a Monte Carlo based planning study was performed describing

the effects of 0.5 and 1.5 T magnetic fields on various clinical proton treatment plans. In total, nine patient plans were simulated across a wide range of tumor sites using the passive or double scattering (DS) technique. Gantry rotation offsets and isocenter shifts were investigated as methods to restore the dose changes to the target volumes as a result of the magnetic field changing the proton beam delivery inside the patient. In summary, small changes in gantry angle and isocenter position were sufficient to restore the dose delivery to essentially that of without a magnetic field. The most heterogeneous case however, a skull-base plan, was also further simulated using pencil beam scanning (PBS) with both single field uniform dose (SFUD) and intensity modulated proton therapy (IMPT). It was reported that the SFUD method indicated the same end result as double scattering, while the IMPT plan did not fully recover dose to the target volume. This was because the IMPT scenario is more complex, with corrections ideally needing to be applied for each individual spot, and/or coupled with optimization. Optimization of the IMPT (PBS) technique was not the focus of that work. The authors did however mention that the PBS method is the more likely method to be implemented in a potential MRI proton therapy system as it could inherently better handle optimization than DS methods.

Finally, in a review paper on emerging proton beam technologies by Schippers and Lomax,³⁹ general discussion is presented which describes the main challenges to face MRI-proton therapy being the interaction of the MRI fields and the proton beam transport magnets and beam monitoring systems.

The general consensus from these works on MRI guided proton therapy is that the proton beam deflection within a patient or water phantom is predictable and so essentially correctable during planning stages. No serious concerns for proton beam deflection via the MRI fringe field have been discussed, in either the inline or perpendicular orientations. Further to this, the beam delivery preference is briefly discussed as being ideally via PBS rather than DS due to the inherent ability of PBS to take advantage of the optimization that the MRI guidance could offer.

In this current work, we investigate the ability of generic proton beams of therapeutic energy to be transported to the isocenter of a 1 T split-bore MRI for the first time. We aim to conclusively describe the impact of the fringe fields from an MRI scanner in both the inline and perpendicular orientation and so fill a void in the current literature. The split-bore MRI is a practical superconducting magnet design based on the Australian MRI-Linac Program which is currently under construction for MRI-Linac research purposes.

2. MATERIALS AND METHODS

2.A. Magnetic modeling and field maps of the MRI design

A fully benchmarked finite element model of the 1 T split-bore MRI system has been reported previously.¹¹ Figure 1 shows a 3D CAD based interpretation of a potential MRI-proton therapy system with magnetic field lines and magnitudes overlayed. In part (a), the inline orientation

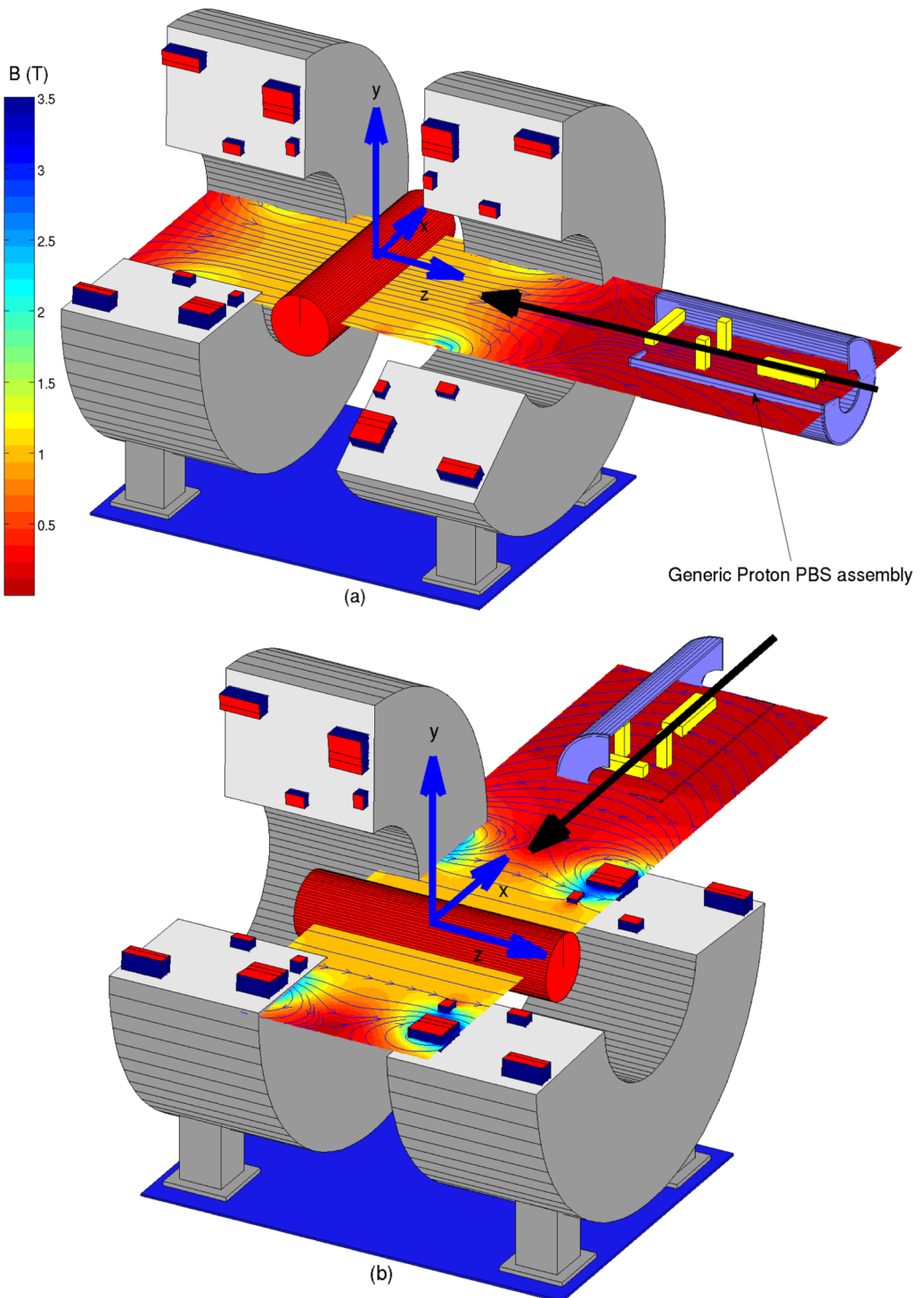


FIG. 1. Three dimensional diagrams of the inline (a) and perpendicular (b) orientations for a potential MRI-guided proton therapy system. A generic proton pencil beam delivery system is shown in each configuration to demonstrate the orientations. This consists of a simple vacuum shield surrounding the scanning magnets and a focussing quadrupole magnet. Note that magnetic flux density and direction overlay is of the default MRI system, i.e., without any external magnetic or ferromagnetic components. In the two orientations, the patient position is indicated by the long cylinder in the MRI bore. The proton beam path is indicated by the large arrow traversing the PBS assembly.

is shown, while in part (b), the perpendicular orientation is detailed. In this figure, a generic proton PBS delivery system is included to aid interpretation of the system setup. Essentially, the inline orientation refers to the proton beam traveling along the z -axis toward the isocenter of the system, which is coincident with the isocenter of the MRI system,

or the diameter spherical volume (DSV). The z -axis is also in the same direction as the main MRI field direction. The perpendicular orientation is when the beam travels along the x -axis toward isocenter. Figure 2 shows a magnetic field contour map from topview of the system and match to the manufacturers' specifications. Also shown in Fig. 2 is a general

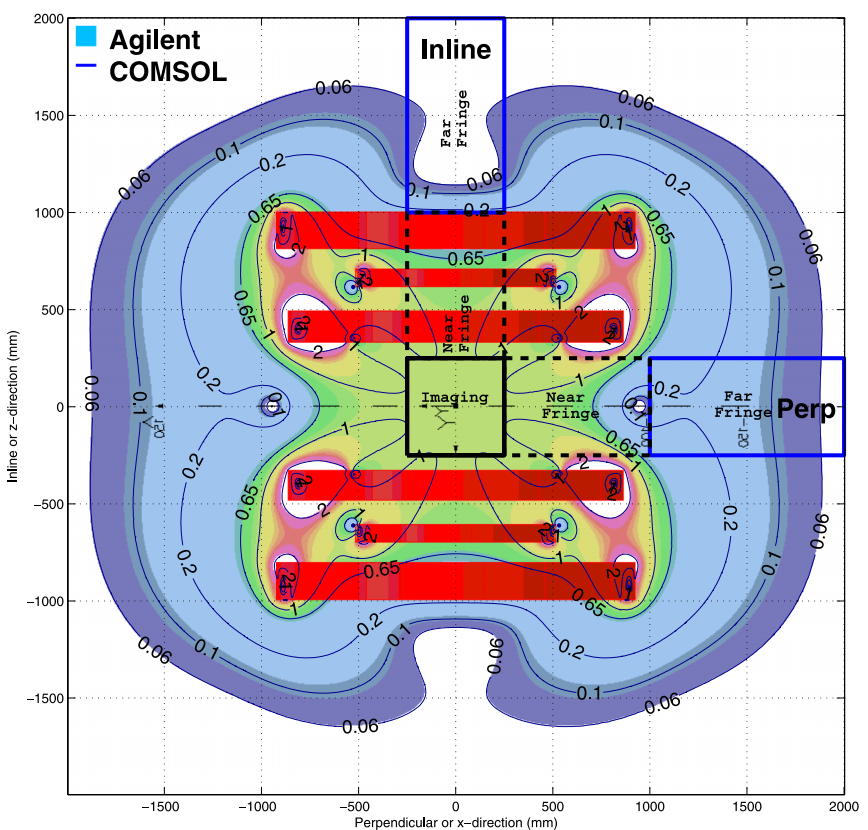


Fig. 2. Top view of the MRI field map; the fill plot displays the manufacturers' model while the contour lines show our COMSOL finite element model. The imaging, near and far fringe fields along the beam CAX for both the inline orientation and perpendicular orientation are outlined. In general, the imaging field is very close to 1 T and comprises almost entirely of a B_z component. The near fringe field encompasses the volumes where the field drops strongly in magnitude from 1 T to around 0.2 T, while the far fringe field is the field from 1 to 5 m from isocenter. The +y direction is out of the page.

classification of the type of magnetic fields that exist in and around the MRI. The imaging field is defined basically as the field which encompasses the patient for imaging. In our definition, this is shown as a $50 \times 50 \times 50 \text{ cm}^3$ volume centered around the isocenter. In this volume, the magnetic field is very uniform in both direction and magnitude, i.e., 1 T in the z -direction. We define the near fringe field as the zone extending from 25 to 100 cm from isocenter. In this region, the magnetic field drops strongly in a roughly linear fashion from 1 T to around 0.2 T in both the inline orientation and perpendicular orientation. Beyond 1 m from isocenter is defined as being the far fringe field.

From the benchmark simulations, look-up-tables (LUT's) of the magnetic field data was exported, one for the inline orientation and one for the perpendicular orientation. The volume of each was $1 \times 1 \times 6 \text{ m}^3$, and contained $101 \times 101 \times 601$ B_x , B_y , and B_z values, that is, at a 10 mm grid spacing. The LUT started at 5 m above isocenter and stopped 1 m below, essentially encompassing the imaging, near and far fringe fields as shown in Fig. 2.

2.B. Monte Carlo simulations

GEANT4 version 10.0.p.02 (Ref. 40) was used for the Monte Carlo modeling. For this particular modeling application, the simulation is entirely for transporting a charged particle through a 3D varying magnetic field. This is because, for

this evaluation study, the simulation volume is considered as a vacuum, and no modulation or collimation of the proton beams was performed.

In essence, this type of simulation could be performed using numerical 2D-symmetric MRI magnetic modeling (B -field calculation) and analytical methods (charged particle transport in a vacuum). Such methods do not work in the case where any part of the proton's paths is nonvacuum, or any ferromagnetic objects exist such as magnetic shielding, bending magnets, or any item required for beam generation or collimation. We have used the full 3D finite element (B -field calculation) and Monte Carlo (charged particle transport in nonvacuum) framework so that real situations can be handled. In this particular study, the choice of using a vacuum with no collimation objects is designed to show the reader the simplest case available—the fundamental underlying proton deflection without complicating geometries or mediums.

The magnetic field implementation inside GEANT4 was taken directly from the advanced example “Purging Magnet” that is part of the software distribution. This allows the simulation of particles through an arbitrary 3D varying magnetic field and has been benchmarked as documented in the example. Implementation in our case required registration of protons and testing of the transport parameters to confirm the paths. Simple sanity checks included ensuring that the protons traveled with a constant radius inside uniform magnetic fields. This step was done by creating uniform LUTs of 0.1, 1,

and 3 T and analyzing the path data. No modification of the default magnetic field specific transport variables (DeltaStep = 0.01 mm, MinEpsilonStep = 5e-05 mm, MaxEpsilonStep = 0.001 mm, DeltaIntersection = 0.001 mm) is required to obtain a radius match to theory as the simulation volume is a vacuum.

The primary variables that would have an impact on this type of simulation are the grid resolution of the 3D LUT and the maximum step length of the protons. In our case, we used 10 mm grid spacing and 1 mm maximum step length. If the grid spacing is too coarse, then the real magnetic field may be under or over estimated in regions of strong gradient change, while if the step length is too large, the deflections will not be calculated accurately as they may miss the changing field values. Various grid spacing and step lengths were tested for our unique 3D LUT. Overall proton deflection paths did not change once the grid spacing became ≤ 10 mm, and the step length ≤ 1 mm. In other words, our sampling of the magnetic field map from the finite element model, and hence subsequent transportation is sufficient at 10 mm resolution.

2.C. Generic proton beams

For the proton particle sources, two types of phase space files were generated. When fired, the particles pass through the isocenter plane with spatial location forming a simple calibration pattern consisting of 1765 protons in total (as shown in Figs. 7–8). The proton energies included 90, 195, and 300 MeV. Graphically, the calibration pattern consists of a single row or line of protons forming a $30 \times 30 \text{ cm}^2$ field outline, cross-hairs at the central axis (CAX), a 9 cm radius circle, and single points at ± 12 cm.

In this initial investigation, we aim to make simple beams with corresponding simple interpretation of the results. Hence, the calibration pattern beams are considered as being fired in a simple particle by particle fashion. There is no time delay or factors involved and they are designed to show simply how protons will deflect based on some given static magnetic field starting properties. Inherently, there is no reason for timing to alter these paths due to MRI-gradient field changes such as during imaging. The magnetic field changes are within mT/m during imaging, which represents less than 0.1% change in the field strength properties.

The first phase space type was designated as a parallel particle source (PPS), where the particle positions inside the phase space matched the calibration pattern, and the momentum directions set to unity in the direction perpendicular to the phase space plane. In other words, when fired, the particles traveled parallel to each other and start at locations as indicated in the calibration pattern. This phase space file was fired from both 5 and 1.5 m from isocenter. The former is designed to detail the natural paths taken by protons as they approach the MRI system, including the different effects of the far fringe, near fringe, and imaging field. The latter will detail proton deflection over the last 1.5 m, a value closer to a clinical broad proton beam as generated by the DS method.

In the second type of phase space file, the particle positions are all collapsed to the CAX, however each particle had a

momentum vector set so that, under no magnetic field, the particles would diverge and pass through the isocenter plane with coordinates matching the calibration pattern. This type of phase space file source was designated as a diverging point source (DPS). This phase space file was fired 1.5 m from the isocenter. This is intended to approximate the PBS proton beam delivery scenario, where a highly monoenergetic pencil beam exits a scanning magnet with spatial location very close to the CAX. For example the IBA Dedicated and Universal Nozzles (IBA Particle Therapy, Louvain-la-Neuve, Belgium) have the lower (y-direction) scanning magnet at 1.94 m from isocenter.⁴¹ The PTC-H system at MD Anderson also appears to have a similar location of the lower scanning magnet (x-direction).⁴²

For all simulations, each phase space was cycled once to generate the proton path data for each energy. In order to analyze, the path deflection data, a simple stepping action argument was implemented inside the Monte Carlo simulation which exported the step properties of each proton to a text file. This file was processed using MATLAB (MathWorks, Natick, MA). Full paths of selected particles were examined, as well as the starting and finishing positions of all particles in the phase space files.

3. RESULTS

3.A. Magnetic field maps

3.A.1. *Inline orientation*

Figure 3 details the magnetic field properties in the inline orientation approach. Part (a) shows a top view of the magnetic flux density extending along the z-axis. Superimposed onto this are the CAX line (along z-axis), a line through $x = 15$ cm, $y = 15$ cm, i.e., offset from the z-axis, and the outline of the 30 cm DSV. In part (b), the corresponding magnetic field components along these two profiles is shown. Along the CAX or z-axis, there is only ever a B_z component to the magnetic field, in other words a proton traveling along this CAX would not experience any magnetic forces. However, once we consider the profile at $x = 15$ cm and $y = 15$ cm, B_x and B_y appear equal and >0 . This is completely expected due to the symmetric nature of the solenoid style magnet. This radial symmetry around the z-axis of the B_x and B_y components will act to rotate protons traveling toward the isocenter around the CAX in a clock-wise direction, as seen from the beams eye view. Further to this, there will be a minor focusing effect toward the CAX. This is analogous to charged particle optics when passing through a solenoid; a charged particle beam will rotate around the CAX and focus.⁴³ We therefore expect that the inline magnetic field will act to rotate our calibration phase space file pattern around the CAX, as well as focus it toward the CAX.

3.A.2. *Perpendicular orientation*

Figure 4 details the magnetic field in the perpendicular orientation approach. Part (a) shows a top view of the magnetic flux density extending along the x-axis. Superimposed onto this are the CAX line (along x-axis), a line through $y = 15$ cm,

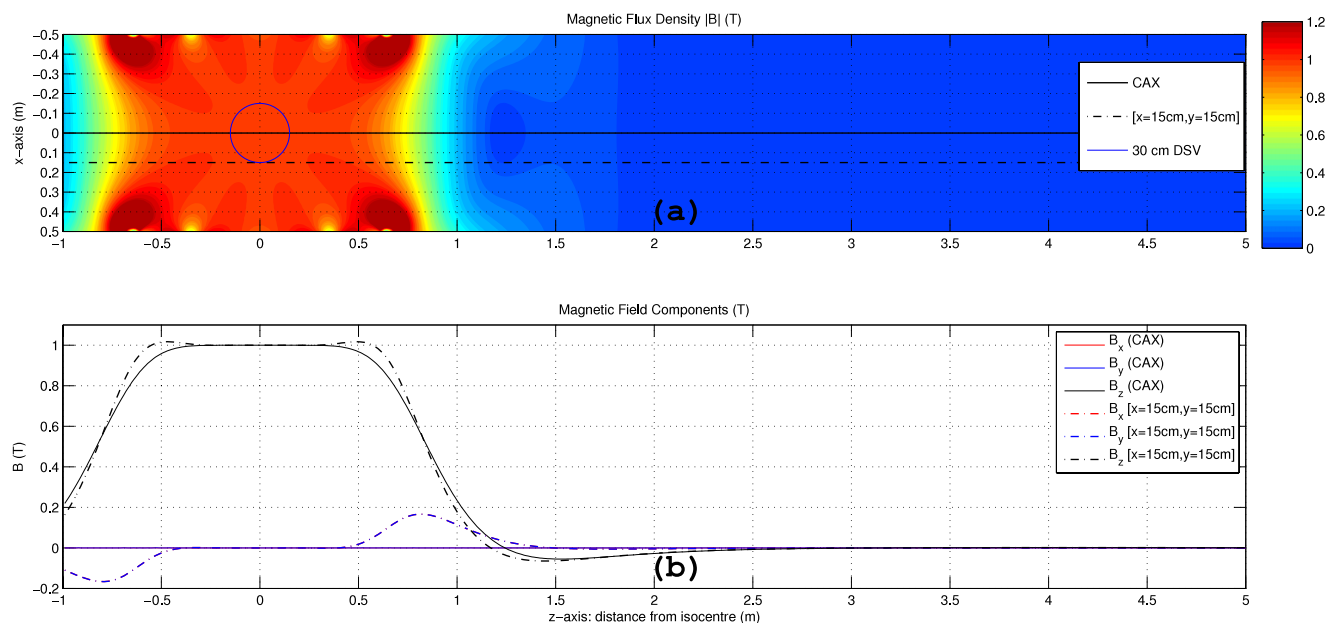


Fig. 3. Details of the magnetic field in the inline orientation approach. (a) Top view of the magnetic flux density extending along the z -axis. (b) Corresponding magnetic field components along the z -axis (CAX) and at 15 cm offset in both the x and y directions. The radial symmetry along this axis is evident by the fact that the B_x and B_y components are equal. Protons traveling along the z -axis (toward isocenter) but offset such as the profile in part (a) ($x = 15$ cm, $y = 15$ cm) will rotate these around the CAX in a clock-wise direction as seen along the beam direction.

$z = 15$ cm, i.e., offset from the x -axis, and the outline of the 30 cm DSV. In part (b), the corresponding magnetic field components along these two profiles is shown.

For a proton beam traveling along the CAX (i.e., the x -axis), the primary deflection component is the B_z component. Interesting to note however, is that the $-B_z$ component ranging from 0.95 m to 5 m from isocenter will deflect protons in

the $-y$ direction, while from 0.95 m to isocenter the opposite will occur. At this point, they enter the strong $+B_z$ component of the near fringe and main MRI imaging field. This will deflect protons in the $+y$ direction, offsetting the initial $-y$ direction deflection. Further to this, a small B_y component is seen in the near fringe field. This will set up smaller deflections in the $\pm x$ -directions. Therefore, we can expect a

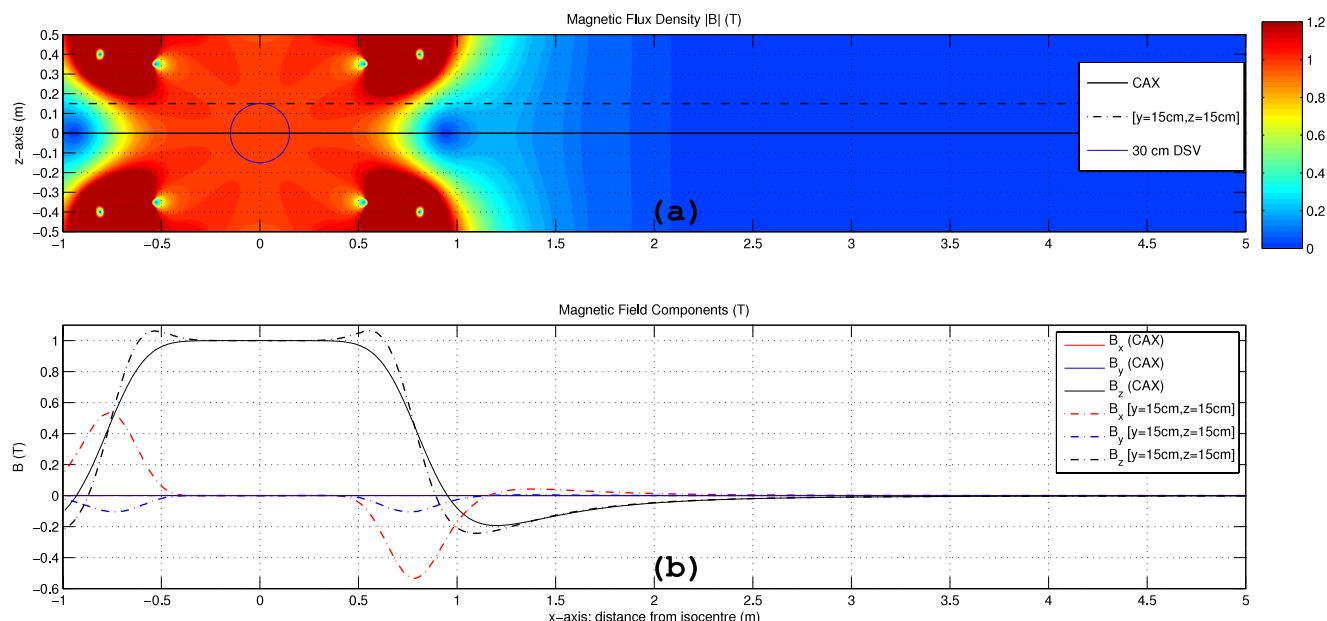


Fig. 4. Details of the magnetic field in the perpendicular orientation approach. (a) Top view of the magnetic flux density extending along the x -axis. (b) Corresponding magnetic field components along the x -axis (CAX) and at 15 cm offset in both the y and z directions. The $-B_z$ component ranging from 0.95 m to 5 m from isocenter will deflect protons in the $-y$ direction. Between 0.95 m and isocenter, they enter the strong $+B_z$ component of the near fringe and main MRI imaging field. This will deflect protons in the $+y$ direction, offsetting the initial $+y$ direction deflection. Further to this, a small B_y component is seen in the near fringe field. This will set up smaller deflections in the $\pm x$ -directions.

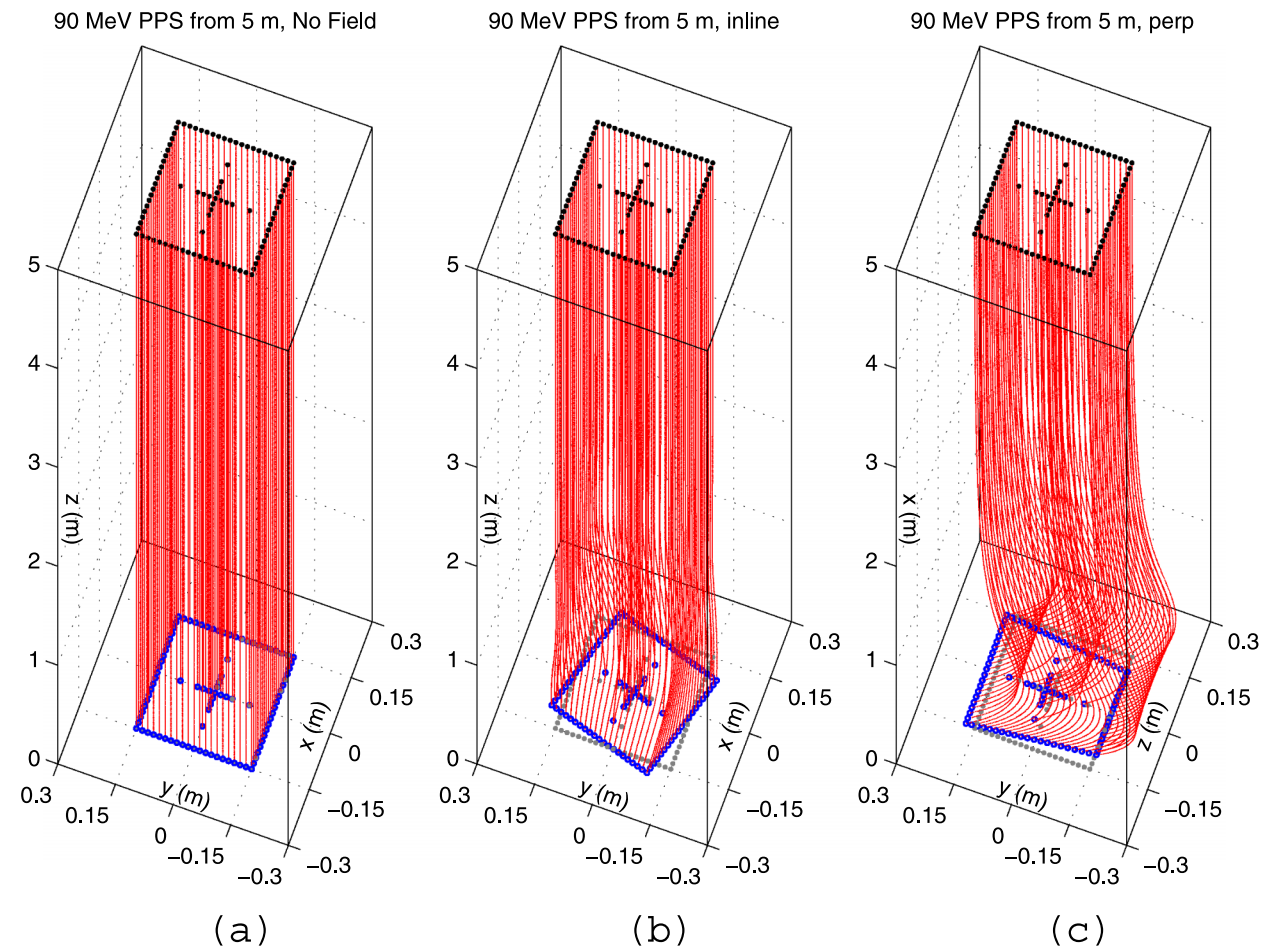


FIG. 5. Proton paths as they travel toward the isocenter of the MRI. (a) No magnetic field. (b) Inline orientation. (c) Perpendicular orientation. The protons were fired from the 90 MeV PPS at 5 m from isocenter. The small dots at the top of each image show the starting positions, the small dots on the x-y plane show the intended positions at isocentre (no magnetic field case), while the large dots on the x-y plane show the actual positions. In total, 97 particles are displayed from the calibration pattern phase space file. As described by the theory of charged particle beams passing through a solenoid style magnet, there is rotation as well as a small focussing effect observed in the inline orientation. While in the perpendicular orientation deflections in both $\pm y$ and $\pm z$ directions are observed. The complex deflection or distortion seen in the perpendicular orientation is attributed to the differences in the magnetic field components between the imaging, near and far fringe fields.

large difference between the deflections seen for the inline orientation and the perpendicular. The phase space calibration pattern will undergo a general shift in one direction in the perpendicular orientation with further distortions seen in the directions perpendicular to the main shift direction. Also, firing the phase space pattern from 1.5 m will differ from at 5 m as the protons will experience a different degree of B_z component, namely, that at 5 m there is the small but long acting $-B_z$ component from 5 to 0.95 m from isocenter.

3.B. Proton beam deflection

3.B.1. Inline orientation

To best illustrate the proton beam deflection, we present 3D plots of the paths of individual protons as they travel from the phase space source and cross the isocenter plane, as well as beams-eye-view diagrams showing the trajectories. Figure 5 shows 3D plots of the paths of 97 protons (selected from a regular 15 mm spaced grid overlaid onto calibration pattern) as they travel from 5 m above isocenter to the isocenter plane.

Part (a) details the nonmagnetic field case while part (b) shows the inline orientation, and further part (c) shows the perpendicular orientation. The particles were fired from the 90 MeV PPS, that is fired parallel. Also shown in the plots are the starting positions, intended stopping positions (no magnetic field) on the isocenter plane, and actual finishing locations as they cross isocenter. Figure 6 shows the same information except that the starting plane is 1.5 m from isocenter, both the PPS and DPS are presented, and the energy is 300 MeV. Figure 7 provides a detailed beams-eye-view of the deflection process.

It is immediately obvious how the calibration pattern has been rotated around the CAX in a clockwise fashion at all energies, and greatest for the lowest energy 90 MeV as expected. The rotations, as gauged from the calibration pattern cross-hairs is 19.0°, 12.8° and 9.8° for the 90, 195, and 300 MeV beams, respectively, when fired from the PPS. The rotation amounts decrease slightly when fired from the DPS, due to the fact that the DPS particles originate at CAX where there is no rotation induced initially. However, once they diverge off-axis the rotation commences.

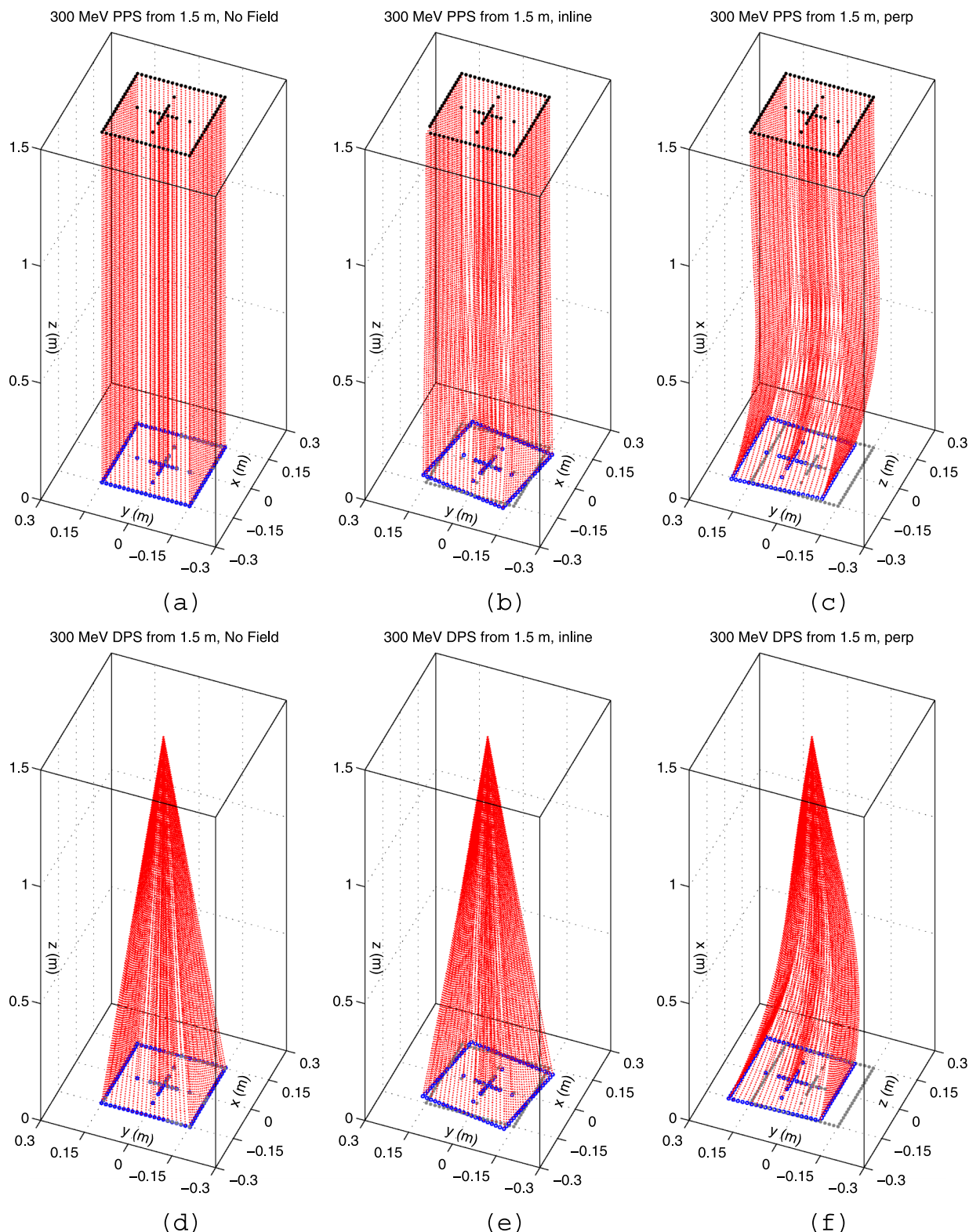


Fig. 6. Similar to Fig. 5 except that the starting position of the phase space file is 1.5 m from the isocenter. In parts (a)–(c), we see particles paths as fired from the 300 MeV PPS phase space file. Parts (d)–(f) details the paths of 300 MeV protons from the DPS. In the inline orientation there is slightly less rotation around the CAX for the DPS, while in the perpendicular orientation there is slightly greater deflection. Figures 7 and 8 details the differences in more detail.

We note that the rotation of the pattern is not linearly related to the energy. The Lorentz force is related to the velocity, and due to relativistic effects the velocity of a 300 MeV proton is only 1.85× higher than a 90 MeV proton.

This approximately matches the observed rotation of these two patterns, namely, that $1.85 \times 9.8^\circ \sim 18.6^\circ$.

Further to this, a small focusing effect is observed, most noticeable at 90 MeV. This is in the order of 1–2 mm focus

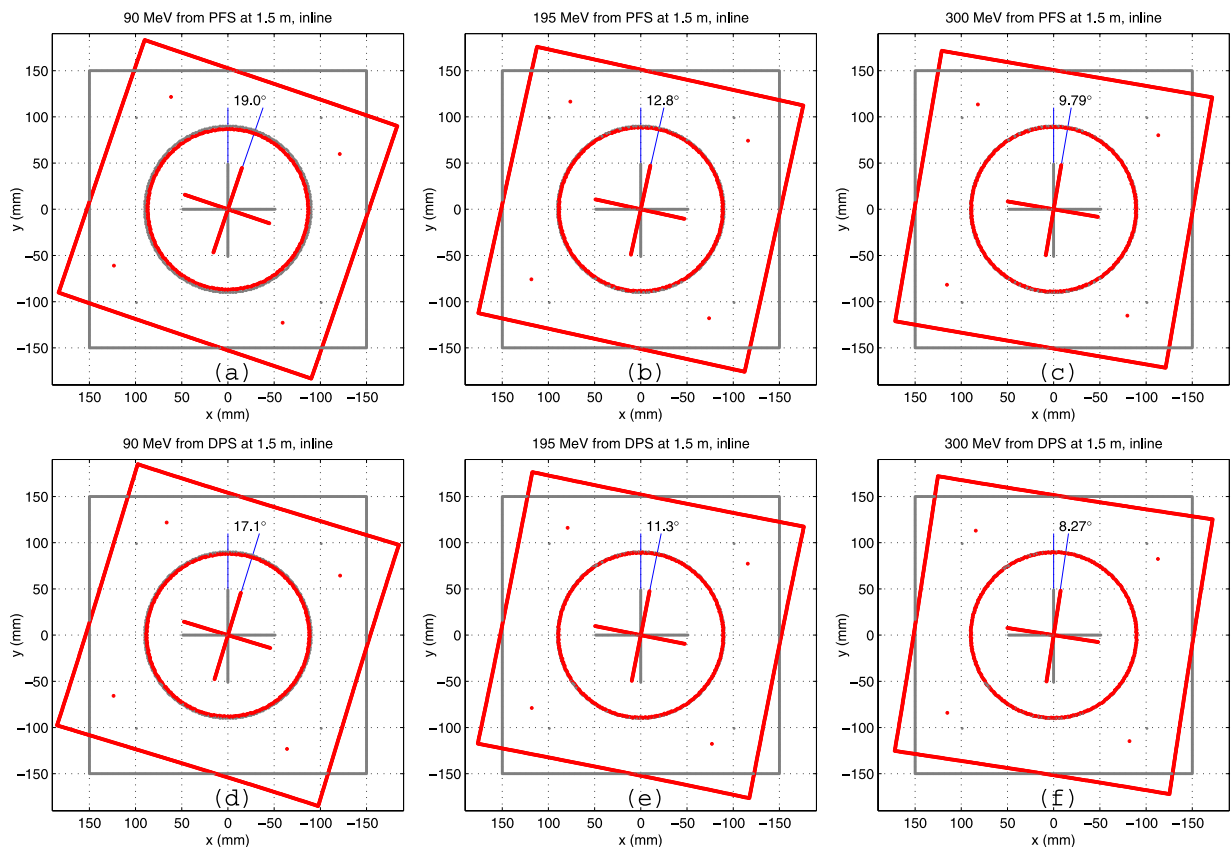


Fig. 7. Beams-eye-view of the proton finishing locations without a magnetic field (small dots) and with a magnetic field (larger dots) in the inline orientation. Parts (a)–(c) show the changes for the PPS phase space files of each energy originating at 1.5 m from isocenter. Parts (d)–(f) repeat the results of (a)–(c) except that the DPS is used.

toward CAX for particles located at 3 cm from CAX, that is, as seen from the perturbation of the circle with 6 cm diameter in the calibration pattern. In general, the deflection of the proton beam calibration pattern, namely, rotation around the CAX and to a lesser extent focusing, confirms the predictions as described in Sec. 2. The results of this section indicate that delivery of a proton pencil beam of a given energy to a precise position on the isocenter plane, with a precise momentum direction, will be possible if three key parameters are known; the starting position, the proton energy, and the momentum direction at the starting position. Reverse engineering, or rather reverse particle transport in a magnetic field, will allow one to determine the exact required starting position and momentum direction of a proton in order for it to hit a desired target. One can quickly reverse the currently presented data and see that in order to deliver a 30×30 cm² flood field of monoenergetic protons to the isocenter (all with a momentum vector that is parallel with the beam CAX) that a continuous range of shifts in proton starting positions and momentum vectors is required.

3.B.2. Perpendicular orientation

Similar to Sec. 3.B.1, results for proton beam deflection in the perpendicular orientation are presented in Figs. 5 and 6 and furthermore in Fig. 8. Part (c) of Fig. 5 shows the

paths taken by 90 MeV protons when fired from the PPS phase space file at 5 m from isocenter. A strong distortion of the calibration pattern is seen, and we can also note that the protons were first deflected in the $-y$ direction before undergoing a stronger deflection in the $+y$ direction. This deflection in the $-y$ direction was predicted by analysis of Fig. 4(b), where the far fringe field contains a mostly $-B_z$ component which then swaps rapidly in direction inside the near fringe and imaging field. However for this proton beam starting at 5 m from isocenter, the strongest overall deflection occurs in the $\pm z$ -directions; basically a focussing of off-axis particles toward the CAX. This is due to the strong off-axis $-B_x$ component in the near fringe field, as shown by the profile at 15 cm in Fig. 4(b).

We next consider the proton beam deflections when fired from 1.5 m above the isocenter, as shown in Fig. 6 parts (c) and (d). In this case, the influence of the far fringe field is mostly removed, the near fringe and imaging field sets up a more consistent general deflection in the $+y$ -direction. Figure 8 details the deflection of the proton calibration maps when viewed from beams-eye-view. Figures 7(a)–7(c) details deflection for the PPS proton beams while Figs. 7(d)–7(f) details that of the DPS. The two beam types clearly result in different distortions. The magnetic field components change strongly over the last 1.5 m to isocenter, as indicated by the profiles shown in Fig. 4 part (b). For all of these patterns,

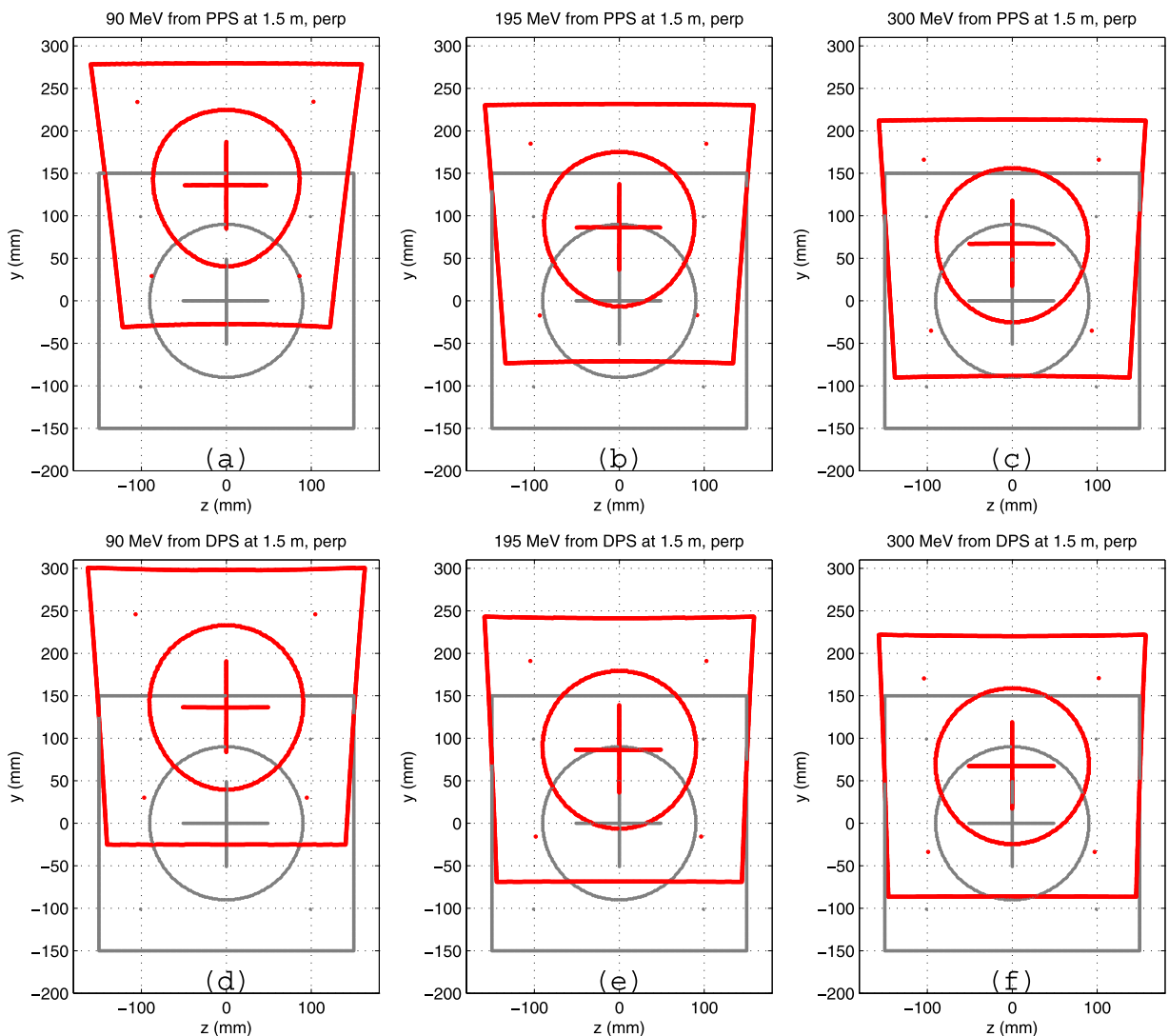


FIG. 8. Similar to Fig. 7 except that the perpendicular orientation is used. Deflection of the PPS particles in the y -direction is generally less, however the distortion in the $\pm z$ -directions is stronger than the DPS. This is simply due to the nonsymmetric nature of the fringe field components and the fact that the DPS particles spend more time nearer to CAX than the PPS particles.

the general deflections in the $+y$ direction arise from the primary B_z component of the near fringe and imaging field. The focusing toward CAX, primarily on the $-y$ side, is caused by the B_x component which rises sharply at about 1.2 m from isocenter to a maximum at 0.8 m from isocenter. It then drops back to zero inside the imaging field, not inducing any more distortion in that direction. In summary, perpendicular ($-x$ direction) deflections of 135, 85, and 65 mm are observed for protons of energy 90, 195, and 300 MeV, respectively, traveling along the CAX. For protons fired at $y = 15$ cm, $z = 15$ cm (off-axis) such as in the PPS the phase space, the deflections are of similar magnitude in the $-x$ direction however a further shift in the z -direction (toward CAX) is seen. There are also subtle differences between the DPS and the PPS deflection patterns; in essence there is greater $+x$ direction deflection when fired from the DPS, however less $\pm z$ (focusing toward CAX) deflection. As seen in Fig. 4(b), the magnetic field components in the near fringe field change quickly as you move away from the CAX. It is this fact that

causes the subtle differences in the deflection and distortion of the calibration pattern when fired from the PPS and DPS.

In summary, a proton beam fired in the perpendicular orientation will undergo significant deflections that depend, similarly to the inline orientation, on the proton starting positions, energy, and momentum directions. Just like the comments made regarding the delivery of parallel flood field in the inline orientation, the perpendicular orientation will require a similar continuous shift in the delivery properties of the protons.

4. DISCUSSION

In this paper, the authors have attempted to address one of the next steps toward MRI-proton therapy: modeling of generic proton beam transport to the treatment zone. Accurate magnetic and Monte Carlo modeling have been employed to predict the impact that a 1 T MRI imaging and fringe field has on the proton paths as they approach the MRI system. Despite being high energy and relatively heavy particles (as

compared to electrons from MRI-Linac interactions), there is still significant distortion of the particle paths. The imaging, near and far fringe field acts to deflect, distort, and rotate proton paths, depending on which approach is taken. It has been predicted previously that a simple gantry offset or patient shift could account for the effects of a transverse field or perpendicular orientation MRI fringe field.²³ This would appear to be entirely true for a single monoenergetic pencil beam, i.e., with calculated offsets it would be possible to deliver a proton pencil beam with a known energy to a known spatial location at isocenter or some point at the patient surface. This type of proton beam delivery is essentially what happens in PBS. Thus, we could expect that proton beam delivery by the PBS technique to be the natural choice for a potential MRI-proton therapy system. The gives further support to the notion first described by Moteabbed *et al.*,³⁸ that the PBS technique would be ideal as it could take advantage of the image guidance offered by the MRI system on a pencil beam-by-beam basis. We note however that as mentioned in Sec. 3.B, the delivery of a broad, monoenergetic, and parallel (to the beam CAX) proton beam to the isocenter plane will require a continuous change in initial momentum directions and starting positions. Delivery from the scanning magnets in PBS will change the starting momentum directions in a timely fashion, however not starting locations. The only apparent way at present would be to rotate the gantry or change on the fly the location of the scanning magnet assembly; both methods would be slow. This notion of having a parallel beam however is not required in practice and is used as an example to demonstrate the complexities of correcting for the impact of the proton beam deflection. It could be predicted that with full inverse planning and magnetic field transport that a desired dose distribution, within a patient specific phantom, could be achieved by a combination of gantry offsets, proton beam energy and momentum direction changes, and patient shifts.

At present, techniques like IMPT typically selects proton energies and positions in a fashion which somewhat paints or accumulates dose to cover the total volume of interest. There are no requirements that this needs to be performed in a manner which is comforting to the human eye. In the case of MRI-guided proton therapy, it may be required that dose be built-up using a time-optimized arrangement of beam delivery parameters, or perhaps even future hardware improvements in scanning magnet design may allow for both precise momentum direction changes as well as location in space as they exit the scanning magnet. In any case, the results of this work indicate that a strong symbiosis is required between the properties of the MRI fringe field and the proton beam delivery system. The proton paths are significantly altered by the fringe field, and correction is required by the beam delivery system which inherently lies inside the MRI fringe field. It is expected that magnetic and Monte Carlo modeling in the potential development of MRI-guided proton beam therapy would continue to play a major role.

As a side point, we note the expected performance of double scattered proton beams where patient specific modulators lie above the patient. First, far from isocenter a range modulator wheel splits up the energies of the primary highly

monoenergetic proton beam. These protons would then travel through the far and near fringe fields before arriving at the patient specific modulator. Without a magnetic field, the protons would have arrived at their intended spatial location, ready for their final energy or range modulation. Based on the results of this work, the impact of an MRI near and far fringe field would be detrimental to the intended beam delivery. Basically, the protons would not arrive as intended at the modulator, and then incorrect final modulation would occur. A simple gantry offset or patient shift will not solve this problem. The distortion caused is related to proton energy and is further dependent on the spatial location of the proton paths. That is, you could correct for a small area of a broad beam only. Every portion of the beam would require different gantry offsets which seems impossible. In essence one could conclude that MRI-guided proton beam therapy would not work with passive or double scattering beam delivery methods. We note however that based on current trends, that most proton therapy machines will likely be of the scanning pencil beam type.

As a final comment, we note that the proton beam deflections observed in this work represent those unique to the particular split-bore 1 T system modeled. Other MRI designs will inherently have different fringe field maps and main field strengths, which will generate different deflection paths from those presented in this work. One aspect of MRI design which would have some impact on the overall proton beam deflection would be to minimize the magnitude and extent of the fringe field. This requirement was in fact a specification of the split-bore design currently presented. There are low fringe field regions (as low as possible from a design perspective) extending from 50 cm from isocentre. Regardless of MRI design, there will remain a strong magnetic field change (both magnitude and direction in 3D) as the main imaging field drops off across the near fringe field. As shown in this work, this zone contributes significantly to the overall deflection. In summary, it can be expected that modeling the proton beam deflection inside a potential MRI-proton therapy system will need to be system specific and a fully benchmarked process. The current work presents a real benchmarked design and serves as a reference for a system without any ferromagnetic components such as shielding or scanning magnets specific to a proton treatment head.

5. CONCLUSION

In this current work, the next steps toward MRI-proton therapy are modeled: transportation of proton beams toward the treatment area of a real MRI system. The proton beam deflections are as predicted previously, of an order that undoubtedly needs some sort of correction. In the inline orientation, a proton beam will exhibit significant rotation around the CAX, and to a much lesser extent some small focussing toward the CAX. In the perpendicular orientation, there are both significant deflection and distortion. Future research efforts may include modeling of full PBS proton beam delivery coupled with magnetic shielding of the scanning magnets, and the development of amelioration strategies to overcome the observed deflections.

ACKNOWLEDGMENTS

The authors acknowledge funding from NHMRC Program Grant No. 1036078 and ARC Discovery Grant No. DP120100821.

^aAuthor to whom correspondence should be addressed. Electronic mail: brad.oborn@gmail.com

- ¹S. Mutic and J. F. Dempsey, "The ViewRay system: Magnetic resonance-guided and controlled radiotherapy," *Semin. Radiat. Oncol.* **24**(3), 196–199 (2014).
- ²J. W. Lagendijk, B. W. Raaymakers, and M. van Vulpen, "The magnetic resonance imaging-linac system," *Semin. Radiat. Oncol.* **24**(3), 207–209 (2014).
- ³B. G. Fallone, "The rotating biplanar Linac-magnetic resonance imaging system," *Semin. Radiat. Oncol.* **24**(3), 200–202 (2014).
- ⁴P. J. Keall, M. Barton, and S. Crozier, "The Australian magnetic resonance imaging-linac program," *Semin. Radiat. Oncol.* **24**(3), 203–206 (2014).
- ⁵J. St. Aubin, S. Steciw, and B. G. Fallone, "Effect of transverse magnetic fields on a simulated in-line 6 MV linac," *Phys. Med. Biol.* **55**(16), 4861–4869 (2010).
- ⁶J. St. Aubin, S. Steciw, and B. G. Fallone, "Waveguide detuning caused by transverse magnetic fields on a simulated in-line 6 MV linac," *Med. Phys.* **37**(9), 4751–4754 (2010).
- ⁷J. St. Aubin, S. Steciw, and B. G. Fallone, "The design of a simulated in-line side-coupled 6 MV linear accelerator waveguide," *Med. Phys.* **37**(2), 466–476 (2010).
- ⁸D. M. Santos, J. S. Aubin, B. G. Fallone, and S. Steciw, "Magnetic shielding investigation for a 6 MV in-line linac within the parallel configuration of a linac-MR system," *Med. Phys.* **39**, 788–797 (2012).
- ⁹D. E. Constantin, L. Holloway, P. J. Keall, and R. Fahrig, "A novel electron gun for inline MRI-linac configurations," *Med. Phys.* **41**(2), 022301 (10pp.) (2014).
- ¹⁰J. Yun, J. St. Aubin, S. Rathee, and B. G. Fallone, "Brushed permanent magnet dc MLC motor operation in an external magnetic field," *Med. Phys.* **37**(5), 2131–2134 (2010).
- ¹¹S. Kolling, B. Oborn, and P. Keall, "Impact of the MLC on the MRI field distortion of a prototype MRI-linac," *Med. Phys.* **40**(12), 121705 (10pp.) (2013).
- ¹²T. Tadic and B. G. Fallone, "Design and optimization of a novel bored biplanar permanent-magnet assembly for hybrid magnetic resonance imaging systems," *IEEE Trans. Magn.* **46**(12), 4052–4058 (2010).
- ¹³T. Tadic and B. G. Fallone, "Three-dimensional nonaxisymmetric pole piece shape optimization for biplanar permanent-magnet MRI systems," *IEEE Trans. Magn.* **47**(1), 231–238 (2011).
- ¹⁴T. Tadic and B. G. Fallone, "Design and optimization of superconducting MRI magnet systems with magnetic materials," *IEEE Trans. Appl. Supercond.* **22**(2), 4400107 (2012).
- ¹⁵F. Liu, S. Crozier, L. Liu, and H. Sanchez-Lopez, "Flanged-edge transverse gradient coil design for a hybrid LINAC-MRI system," *J. Magn. Reson.* **226**, 70–78 (2013).
- ¹⁶B. Burke, K. Wachowicz, B. G. Fallone, and S. Rathee, "Effect of radiation induced current on the quality of MR images in an integrated linac-MR system," *Med. Phys.* **39**(10), 6139–6147 (2012).
- ¹⁷B. Burke, A. Ghila, B. G. Fallone, and S. Rathee, "Radiation induced current in the RF coils of integrated linac-MR systems: The effect of buildup and magnetic field," *Med. Phys.* **39**(8), 5004–5014 (2012).
- ¹⁸B. W. Raaymakers, A. J. E. Raaijmakers, A. N. T. J. Kotte, D. Jette, and J. J. W. Lagendijk, "Integrating a MRI scanner with a 6 MV radiotherapy accelerator: Dose deposition in a transverse magnetic field," *Phys. Med. Biol.* **49**, 4109–4118 (2004).
- ¹⁹A. J. E. Raaijmakers, B. W. Raaymakers, and J. J. W. Lagendijk, "Integrating a MRI scanner with a 6 MV radiotherapy accelerator: Dose increase at tissue-air interfaces in a lateral magnetic field due to returning electrons," *Phys. Med. Biol.* **50**, 1363–1376 (2005).
- ²⁰A. J. E. Raaijmakers, B. W. Raaymakers, S. van der Meer, and J. J. W. Lagendijk, "Integrating a MRI scanner with a 6 MV radiotherapy accelerator: Impact of the surface orientation on the entrance and exit dose due to the transverse magnetic field," *Phys. Med. Biol.* **52**, 929–939 (2007).
- ²¹A. J. E. Raaijmakers, B. W. Raaymakers, and J. J. W. Lagendijk, "Experimental verification of magnetic field dose effects for the MRI-accelerator," *Phys. Med. Biol.* **52**, 4283–4291 (2007).
- ²²C. Kirkby, T. Stanescu, S. Rathee, M. Carbone, B. Murray, and B. G. Fallone, "Patient dosimetry for hybrid MRI-radiotherapy systems," *Med. Phys.* **35**(3), 1019–1027 (2008).
- ²³A. J. E. Raaijmakers, B. W. Raaymakers, and J. J. W. Lagendijk, "Magnetic-field-induced dose effects in mr-guided radiotherapy systems: Dependence on the magnetic field strength," *Phys. Med. Biol.* **53**(4), 909–923 (2008).
- ²⁴C. Kirkby, T. Stanescu, and B. G. Fallone, "Magnetic field effects on the energy deposition spectra of MV photon radiation," *Phys. Med. Biol.* **54**, 243–257 (2009).
- ²⁵B. M. Oborn, P. E. Metcalfe, M. J. Butson, and A. B. Rosenfeld, "High resolution entry and exit Monte Carlo dose calculations from a linear accelerator 6 MV beam under influence of transverse magnetic fields," *Med. Phys.* **36**(8), 3549–3559 (2009).
- ²⁶B. M. Oborn, P. E. Metcalfe, M. J. Butson, and A. B. Rosenfeld, "Monte Carlo characterization of skin doses in 6 MV transverse field MRI-linac systems: Effect of field size, surface orientation, magnetic field strength, and exit bolus," *Med. Phys.* **37**(10), 5208–5217 (2010).
- ²⁷T. C. F. van Heijst, M. D. den Hartogh, J. J. W. Lagendijk, H. J. G. Desirée van den Bongard, and B. van Asselen, "MR-guided breast radiotherapy: Feasibility and magnetic-field impact on skin dose," *Phys. Med. Biol.* **58**(17), 5917–5930 (2013).
- ²⁸B. M. Oborn, P. E. Metcalfe, M. J. Butson, A. B. Rosenfeld, and P. J. Keall, "Electron contamination modeling and skin dose in 6 MV longitudinal field MRIgRT: Impact of the MRI and MRI fringe field," *Med. Phys.* **39**(2), 874–890 (2012).
- ²⁹A. Keyvanloo, B. Burke, B. Warkentin, T. Tadic, S. Rathee, C. Kirkby, D. M. Santos, and B. G. Fallone, "Skin dose in longitudinal and transverse linac-MRIs using Monte Carlo and realistic 3D MRI models," *Med. Phys.* **39**(10), 6509–6521 (2012).
- ³⁰B. M. Oborn, S. Kolling, P. E. Metcalfe, S. Crozier, D. W. Litzenberg, and P. J. Keall, "Electron contamination modeling and reduction in a 1 T open bore inline MRI-linac system," *Med. Phys.* **41**(5), 051708 (15pp.) (2014).
- ³¹I. Meijzing, B. W. Raaymakers, A. J. E. Raaijmakers, J. G. M. Kok, L. Hogeweg, B. Liu, and J. J. W. Lagendijk, "Dosimetry for the MRI accelerator: The impact of a magnetic field on the response of a Farmer NE2571 ionization chamber," *Phys. Med. Biol.* **54**, 2993–3002 (2009).
- ³²K. Smit, B. van Asselen, J. G. M. Kok, A. H. L. Aalbers, J. J. W. Lagendijk, and B. W. Raaymakers, "Towards reference dosimetry for the MR-linac: Magnetic field correction of the ionization chamber reading," *Phys. Med. Biol.* **58**(17), 5945–5957 (2013).
- ³³K. Smit, J. G. M. Kok, J. J. W. Lagendijk, and B. W. Raaymakers, "Performance of a multi-axis ionization chamber array in a 1.5 T magnetic field," *Phys. Med. Biol.* **59**(7), 1845–1855 (2014).
- ³⁴M. Reynolds, B. G. Fallone, and S. Rathee, "Dose response of selected ion chambers in applied homogeneous transverse and longitudinal magnetic fields," *Med. Phys.* **40**(4), 042102 (7pp.) (2013).
- ³⁵M. Reynolds, B. G. Fallone, and S. Rathee, "Dose response of selected solid state detectors in applied homogeneous transverse and longitudinal magnetic fields," *Med. Phys.* **41**(9), 092103 (12pp.) (2014).
- ³⁶B. W. Raaymakers, A. J. E. Raaijmakers, and J. J. W. Lagendijk, "Feasibility of MRI guided proton therapy: Magnetic field dose effects," *Phys. Med. Biol.* **53**(20), 5615–5622 (2008).
- ³⁷R. Wolf and T. Bortfeld, "An analytical solution to proton bragg peak deflection in a magnetic field," *Phys. Med. Biol.* **57**(17), N329–N337 (2012).
- ³⁸M. Moteabbed, J. Schuemann, and H. Paganetti, "Dosimetric feasibility of real-time MRI-guided proton therapy," *Med. Phys.* **41**(11), 111713 (11pp.) (2014).
- ³⁹J. M. Schippers and A. J. Lomax, "Emerging technologies in proton therapy," *Acta Oncol.* **50**(6), 838–850 (2011).
- ⁴⁰S. Agostinelli *et al.*, "GEANT4—A simulation toolkit," *Nucl. Instrum. Methods Phys. Res. A* **506**, 250–303 (2003).
- ⁴¹J. B. Farr, F. Dessy, O. De Wilde, O. Bietzer, and D. Schönenberg, "Fundamental radiological and geometric performance of two types of proton beam modulated discrete scanning systems," *Med. Phys.* **40**(7), 072101 (8pp.) (2013).
- ⁴²S. W. Peterson, J. Polf, M. Bues, G. Ciangaru, L. Archambault, S. Beddar, and A. Smith, "Experimental validation of a Monte Carlo proton therapy nozzle model incorporating magnetically steered protons," *Phys. Med. Biol.* **54**(10), 3217–3229 (2009).
- ⁴³V. Kumar, "Understanding the focusing of charged particle beams in a solenoid magnetic field," *Am. J. Phys.* **77**(8), 737–741 (2009).